Original Investigation

Prostate Cancer Detection Using Computed Very High b-value Diffusion-weighted Imaging: How High Should We Go?

Andrew B. Rosenkrantz, MD, Nainesh Parikh, MD, Andrea S. Kierans, MD*, Max Xiangtian Kong, MD**, James S. Babb, PhD, Samir S. Taneja, MD, Justin M. Ream, MD

Rationale and Objectives: The aim of this study was to assess prostate cancer detection using a broad range of computed b-values up to 5000 s/mm^2.

Materials and Methods: This retrospective Health Insurance Portability and Accountability Act-compliant study was approved by an institutional review board with consent waiver. Forty-nine patients (63 ± 8 years) underwent 3T prostate magnetic resonance imaging before prostatectomy. Examinations included diffusion-weighted imaging (DWI) with b-values of 50 and 1000 s/mm^2. Seven computed DWI image sets (b-values: 1000, 1500, 2000, 2500, 3000, 4000, and 5000 s/mm^2) were generated by mono-exponential fit. Two blinded radiologists (R1 [attending], R2 [fellow]) independently evaluated diffusion weighted image sets for image quality and dominant lesion location. A separate unblinded radiologist placed regions of interest to measure tumor-to-peripheral zone (PZ) contrast. Pathologic findings from prostatectomy served as reference standard. Measures were compared between b-values using the Jonckheere-Terpstra trend test, Spearman correlation coefficient, and generalized estimating equations based on logistic regression for correlated data.

Results: As b-value increased, tumor-to-PZ contrast and benign prostate suppression for both readers increased ($r = +0.65$ to $+0.71$, $P \leq 0.001$), whereas anatomic clarity, visualization of the capsule, and visualization of peripheral-transition zone edge decreased ($r = -0.69$ to -0.75, $P \leq 0.003$). Sensitivity for tumor was highest for R1 at b1500–3000 (84%–88%) and for R2 at b1500–2500 (70%–76%). Sensitivities for both pathologic outcomes were lower for both readers at both b1000 and the highest computed b-values. Sensitivity for Gleason >6 tumor was highest for R1 at b1500–3000 (90%–93%) and for R2 at 1500–2500 (78%–80%). The positive predictive value for tumor for R1 was similar from b1000 to 4000 (93%–98%) and for R2 was similar from b1500 to 4000 (88%–94%).

Conclusions: Computed b-values in the range of 1500–2500 s/mm^2 (but not higher) were optimal for prostate cancer detection; b-values of 1000 or 3000–5000 exhibited overall lower performance.

Key Words: Prostate; neoplasms; magnetic resonance imaging; diffusion magnetic resonance imaging; imaging.

© 2016 The Association of University Radiologists. Published by Elsevier Inc. All rights reserved.

INTRODUCTION

Diffusion-weighted imaging (DWI) plays a central role in prostate magnetic resonance imaging (MRI) interpretation, being designated as the dominant sequence for guiding localization and risk assessment of focal peripheral zone (PZ) lesions in the American College of Radiology Prostate Imaging Reporting and Data System (PI-RADS) version 2 guidelines (1). When performing DWI using conventional b-values up to 1000 s/mm^2, the apparent diffusion coefficient (ADC) map serves as the primary image set for interpretation. In comparison, unsuppressed signal within benign prostate tissue obscures potential hyperintensity within tumors on the acquired DWI at such b-values (2). Although higher b-value DWI yields greater benign tissue suppression and thus potential improved tumor visualization, direct acquisition of such b-values is technically difficult because of issues related to reduced signal-to-noise ratio (SNR) and increased anatomic distortion and artifacts resulting from increased eddy currents at these b-values (3).

A number of studies report techniques entailing novel pulse sequences and parameter optimization for improving distortion and artifacts of high b-value DWI (4–6). However, an

Acad Radiol 2016; 23:704–711

From the Department of Radiology, NYU School of Medicine, NYU Langone Medical Center, 550 First Avenue, New York, NY 10016 (A.B.R., N.P., A.S.K., J.S.B., J.M.R.); Department of Pathology (M.X.K.); Department of Urology, Division of Urologic Oncology, NYU School of Medicine, NYU Langone Medical Center, New York, New York (S.S.T.). *Current address: Department of Radiology, Weill Cornell Medical College, New York, NY. **Current address: Pathology Consultants of New Mexico, Roswell, New Mexico. Received October 22, 2015; revised January 29, 2016; accepted February 1, 2016. **Support**: This study was supported by the Joseph and Diane Steinberg Charitable Trust. **Address correspondence to:** A.B.R. e-mail: Andrew.Rosenkrantz@nyumc.org

© 2016 The Association of University Radiologists. Published by Elsevier Inc. All rights reserved.
http://dx.doi.org/10.1016/j.acra.2016.02.003

alternative approach is to perform "computed" DWI, in which the very high b-value images are mathematically derived from the ADC map without being actually acquired themselves (7). This scheme is intended to provide the benign prostate signal suppression of acquired very high b-value images while avoiding the challenges of low SNR and increased artifacts that are encountered when directly acquiring such images. Although computed high b-value DWI does not acquire additional diffusion data compared to the standard b-values, this post-processing technique may in practice improve visual conspicuity of tumors, without requiring any increase in scan time. Indeed, a number of studies have demonstrated significantly improved prostate cancer detection using computed b-values up to 2000 (3,8–10). Furthermore, PI-RADS v2 formally acknowledges the role of computed DWI in multiparametric prostate MRI and incorporates findings at the very high b-values into its lesion assessment categories (1).

Although the initial literature relating to computed DWI in the prostate generated images at b-values up to 2000, such a b-value need not serve as an upper limit, as continual greater degrees of benign tissue suppression occur as the b-value increases even further. In fact, one recent study explored computed DWI of the prostate at b-values up to 4000 (11), reporting greatest signal contrast between tumor and benign prostate at the highest investigated b-value of 4000. Although the findings appear promising, that earlier study included a small sample size of only 14 patients, employed ultrasound-guided biopsy as the reference standard, and did not compare actual reader accuracy for tumor detection between the various b-values (11). Given such limitations, the added clinical value of b-values in the investigated range remains unknown, and further investigation is warranted. Therefore, in this study, our aim is to assess prostate cancer detection using a broad range of computed b-values ranging from 1000 to 5000s/mm^2.

METHODS

Patients

This retrospective study was Health Insurance Portability and Accountability Act-compliant and was approved by our institutional review board, receiving a waiver of the requirement for written informed consent. Initially, 56 consecutive patients who underwent multiparametric MRI of the prostate before radical prostatectomy were identified. Patients were then excluded for the following reasons: MRI performed at an outside institution ($n = 4$), MRI performed at 1.5T ($n = 2$), and severe artifact on DWI ($n = 1$). These exclusions left a final included cohort of 49 patients (mean age: 63 ± 8 years). MRI was performed in these patients for the following reasons: no prior biopsy ($n = 9$), prior negative biopsy with persistent clinical concern for prostate cancer ($n = 5$), and prior positive biopsy ($n = 37$). In patients who had undergone prior biopsy before MRI, the mean delay between biopsy and MRI was 383 ± 757 days. The mean delay between MRI and surgery was 62 ± 67 days. The mean prostate specific antigen level was 6.4 ± 4.4 ng/mL.

MRI Acquisition and Post-processing

MRI was performed in all patients using a 3T clinical system and a multichannel pelvic phased-array coil (MAGNETOM Trio, Biograph, or Skyra, Siemens Healthcare, Erlangen, Germany; 6, 12, or 18 coil channels, respectively). All examinations included an axial turbo spin echo T2-weighted imaging (T2WI) sequence of the prostate and seminal vesicles [repetition time (TR)/echo time (TE) of 4000–4960/105 ms, slice thickness of 3 mm, field of view of 180 × 180 mm, matrix of 256 × 256, parallel imaging factor 2, 3 averages], as well as an axial single-shot fat-suppressed echo-planar imaging DWI sequence of the prostate and seminal vesicles (TR/TE of 4100/86 ms, slice thickness of 3 mm, field of view of 200 × 200 mm, matrix of 100 × 220, parallel imaging factor 2, 10 signal averages per b-value; b-values of 50 and 1000 s/mm^2), as has been previously published (12). The ADC map was constructed by the console in an inline fashion on a voxel-by-voxel basis using a standard mono-exponential fit. Coronal T2WI, dynamic contrast-enhanced imaging of the prostate, and delayed post-contrast fat-suppressed T1-weighted imaging of the pelvic were also performed for all examinations for all MRI systems, although these were not evaluated as part of this study. Simultaneous position emission tomography (PET) was not performed in patients imaged using the Biograph.

At the time of this investigation, dedicated post-processing software (ProFuse, Eigen, Grass Valley, CA) was used to construct seven computed DWI image sets for each examination at the following b-values—1000, 1500, 2000, 2500, 3000, 4000, and 5000 s/mm^2—based on a mono-exponential model. A greater number of b-values was selected in the lower portion of this range given that these lower b-values more closely correspond with the b-values used in current clinical practice. The post-processing software assigned only non-negative voxel values for computed DWI, consistent with the magnitude reconstruction of acquired DWI in clinical practice.

Image Interpretation

Two radiologists (JR and AK with 2- and 1-year experience in prostate MRI, and having reviewed approximately 500 and 250 prostate MRI examinations prior to this study, respectively) independently evaluated the ADC map, the acquired b1000 images, and the six computed DWI image sets for each patient, blinded to clinical and pathologic information aside from the knowledge that each patient had undergone radical prostatectomy. All image sets were initially assigned a unique identifier in order to be blinded in terms of both patient identity and b-value (aside from the ADC map, for which only the patient identity was blinded). The seven computed b-value image sets (1000 through 5000 s/mm^2) and the ADC maps were then individually evaluated in a random order in terms

of both of these factors. The readers were able to freely adjust the window and level settings of each individual image set at the time of interpretation. Each distinct DWI image set was reviewed simultaneously with the axial T2WI, which had been replicated a sufficient number of times in order to be separately associated with each image set for each patient. Using this approach, during each assessment, readers reviewed T2WI in combination with a single computed b-value (1000 through 5000 s/mm^2) or the ADC map, blinded to the other image sets. The directly acquired b1000 image set was not included in the analysis, so as to solely compare computed DWI of varying b-values. The T2WI was used only as an anatomic reference, with the readers' interpretations reflecting solely abnormalities identified on the given DWI image set.

For computed b-value image sets, the readers first evaluated the image set using a 1–5 scale for various measures of subjective image quality: background signal suppression of the prostate (5 = maximal signal suppression), anatomic clarity (5 = excellent clarity), visualization of the prostatic capsule (5 = excellent visualization), and visualization of the peripheral-transition zone (TZ) boundary (5 = excellent visualization). Then, for all image sets, the readers identified the dominant visualized lesion using the given image set, considered to be an area exhibiting focal increased signal intensity (or decreased voxel values when evaluating an ADC map). If multiple lesions showing increased signal intensity (or decreased voxel values for the ADC map) were identified, then the readers selected only a single area based on consideration of the lesion's size, focality, and degree of signal alteration. The readers recorded for each selected lesion its laterality, slice position, and location within either the anterior versus posterior and medial versus lateral aspect of the prostate. The readers had the option to select no suspicious lesion for a given image set if no area of abnormal signal intensity (SI) could be identified. Also, for each identified lesion, the readers recorded using a 1–5 scale the lesion's degree of visual conspicuity (5 = excellent conspicuity) and their degree of confidence in the lesion (5 = very high confidence).

One month following the initial interpretations, one of the two radiologists (JR) evaluated all image sets using additional post-processing software (FireVoxel; https://wp.nyu.edu/firevoxel/), aware of pathologic findings. The radiologist manually traced a region of interest (ROI) within an identified abnormality on the ADC map for each patient corresponding with the location of the pathologically defined index tumor, as subsequently described, aside from two patients in whom no corresponding abnormality could be identified during retrospective unblinded evaluation. The ROI was traced just within the outer edge of the lesion. A similar-sized ROI was also placed in an area of normal-appearing PZ that was benign on histologic assessment. The software was then used to directly copy the ROIs to all of the b-value images. The mean value of all ROIs was recorded. Tumor-to-PZ contrast was then calculated as $(SI_{tumor} - SI_{PZ})/(SI_{tumor} + SI_{PZ})$, giving a value between 0 and 1 and that is greater in the setting of higher relative contrast (13,14). Mean ROI size was 0.85 ± 0.69 cm^2 and the range was 0.07–4.30 cm^2.

Reference Standard

The prostatectomy specimens underwent fine-needle formalin injection followed by 24-hour fixation. Standard 4-μm step-section slides using H&E staining were then prepared of the specimens in their entirety. The slides for each specimen were reviewed by one of three institutional uropathologists using a standardized diagram of the prostate for recording the location, size, and Gleason score of all tumor foci. For each patient, the index tumor was selected as the tumor focus having the highest Gleason score. If multiple tumor foci shared the highest Gleason score, then the largest of these foci was selected as the index tumor. An index tumor was identified for all patients.

An additional radiologist (AR, with 7 years of experience in prostate MRI) compared the radiologists' MRI readings and the standardized prostate diagrams constructed by the pathologists in order to compare the assigned locations of the identified suspicious lesion on MRI and the index tumor identified on pathologic assessment. Lesions were considered to be a match when occurring within the same position of the prostate in terms of all evaluated location attributes (right vs left, medial vs lateral within the given lobe, base vs midgland vs apex, and anterior vs posterior).

Statistics

All analyses were performed separately for the two readers. The subjective image quality measures were assessed for a generic monotonic trend across b-values using the Jonckheere-Terpstra (JT) trend test, and the Spearman rank correlation coefficient was used to characterize the strength of such monotonic associations. In order to fulfill the assumption of the JT test of independent samples (implying that each subject provides data for a single b-value), the sample of 49 subjects was randomly partitioned into 7 disjoint subgroups of 7 subjects each, and the subgroups were randomly assigned to the 7 b-value, thereby creating proper subsets wherein no one subject provided data for more than one b-value. The JT test was then applied to these subsets. This approach was applied across b-values ranging from 1000 through 5000 s/mm^2 for background suppression, anatomic clarity, visualization of the capsule, visualization of the PZ/TZ edge, and tumor-to-PZ contrast, s/mm^2. Inter-reader agreement for the subjective features was computed by combining each reader's assessments for all b-values into a single vector and computing weighted kappa coefficients. Logistic regression for correlated data was used to compare the image sets with respect to sensitivity and the positive predictive value (PPV) for the detection of the index tumor relative to pathology as reference standard. Logistic regression for correlated data was also used to compare image sets with respect to the sensitivity for detection of tumors with Gleason score ≥7 relative to pathology. Specifically, generalized estimating equation (GEE) based on binary logistic regression was used to model concordance between reader interpretation and results from pathology as a function of image

set. This model accounted for statistical dependencies among results provided for the same subject. GEE avoids potentially erroneous assumptions of the more conventional general linear mixed model and may therefore provide more reliable estimates of associations among model variables (15). The analysis required a difference in interpretation of at least 25% of cases in order to achieve 80% power to detect a difference in sensitivity of 10% between any given combination of two DWI image sets. All statistical tests were conducted at the two-sided 5% significance level using SAS 9.3 (SAS Institute, Cary, NC).

RESULTS

Image Quality

Background prostate tissue suppression showed a significant increase with increasing b-value for both readers ($r = +0.65$ to $+0.71$, $P \leq 0.001$) (Table 1). However, anatomic clarity, visualization of the capsule, and visualization of the peripheral-transition zone boundary all showed significant decreases with increasing b-value readers ($r = -0.69$ to -0.75, $P \leq 0.003$) (Table 1). Inter-reader agreement was moderate for all of these features (background prostate tissue suppression: 0.412; anatomic clarity: 0.532; visualization of the capsule: 0.527; visualization of the peripheral-transition zone boundary: 0.507).

Pathologic Findings

The distribution of Gleason scores of the index tumor in the 49 patients was as follows: 3 + 3 ($n = 9$), 3 + 4 ($n = 30$), 4 + 3 ($n = 2$), 4 + 4 (4), 4 + 5 ($n = 3$), and 5 + 5 ($n = 1$). Thirty-six were located primarily in the PZ, and 13 were located primarily in the TZ. The mean tumor diameter was 17 ± 8 mm. Extraprostatic extension was present in 12 patients and seminal vesicle invasion in one patient.

Tumor Detection

Tables 2 and 3 summarize and compare tumor detection using the various image sets for both readers. The highest sensitivity for tumor was achieved at b-values of 1500–3000 for reader 1 and of 1500–2500 for reader 2, and for Gleason score ≥7 tumor at b-values of 1500–3000 for reader 1 and of 1500–2500 for reader 2. Sensitivities for both pathologic outcomes were lower for both readers at a b-value of 1000 as well as at the highest computed b-values. Reader 1 achieved significantly higher sensitivity for Gleason ≥7 tumor at b-values of

TABLE 1. Comparison of Measures of Image Quality Between Diffusion-weighted Images Using Various b-values (Provided as Mean ± Standard Deviation)

	Background Suppression		Anatomic Clarity		Visualization of Capsule		Visualization of PZ-TZ Edge	
b-Value	Reader 1	Reader 2	Reader 1	Reader 2	Reader 1	Reader 2	Reader 1	Reader 2
1000	2.29 ± 0.71	2.37 ± 0.86	4.53 ± 0.65	4.65 ± 0.75	4.69 ± 0.51	4.69 ± 0.74	4.49 ± 0.77	4.33 ± 0.77
1500	3.08 ± 0.81	3.49 ± 0.82	3.82 ± 0.39	3.90 ± 0.42	4.14 ± 0.68	3.80 ± 0.50	3.67 ± 0.63	3.98 ± 0.80
2000	3.55 ± 0.54	4.20 ± 0.54	3.63 ± 0.49	3.06 ± 0.24	3.80 ± 0.46	3.31 ± 0.47	2.98 ± 0.32	3.04 ± 0.20
2500	3.63 ± 0.57	4.59 ± 0.61	3.00 ± 0.29	2.71 ± 0.46	3.12 ± 0.33	2.98 ± 0.14	3.29 ± 0.76	2.71 ± 0.50
3000	3.67 ± 0.72	4.90 ± 0.31	2.84 ± 0.37	2.37 ± 0.53	3.04 ± 0.41	2.61 ± 0.53	2.80 ± 0.91	2.41 ± 0.67
4000	4.43 ± 0.65	4.94 ± 0.43	2.59 ± 0.57	1.55 ± 0.54	2.90 ± 0.42	1.80 ± 0.46	2.18 ± 0.91	1.39 ± 0.53
5000	4.35 ± 1.01	4.49 ± 1.32	2.45 ± 1.12	2.35 ± 1.88	2.76 ± 0.90	2.16 ± 1.52	1.94 ± 0.90	2.10 ± 1.58

PZ-TZ, peripheral zone-transition zone.

TABLE 2. Comparison of Diagnostic Performance for Index Tumor Localization and Tumor-to-peripheral Zone (PZ) Contrast Between Various Diffusion-weighted Image Sets

	Sensitivity (All Tumors)		Sensitivity (Gleason score > 6)		PPV		Tumor-to-PZ
b-Value	Reader 1	Reader 2	Reader 1	Reader 2	Reader 1	Reader 2	Contrast
ADC map	81.6% (40/49)	71.4% (35/49)	82.5% (33/40)	75.0% (30/40)	95.2% (40/42)	85.4% (35/41)	0.18 ± 0.08
1000	79.6% (39/49)	63.3% (31/49)	80.0% (32/40)	67.5% (27/40)	95.1% (39/41)	82.1% (32/39)	0.18 ± 0.13
1500	85.7% (42/49)	75.5% (37/49)	92.5% (37/40)	80.0% (32/40)	93.3% (42/45)	92.5% (37/40)	0.25 ± 0.16
2000	87.8% (43/49)	71.4% (35/49)	92.5% (37/40)	77.5% (31/40)	95.6% (43/45)	87.5% (35/40)	0.33 ± 0.18
2500	85.7% (42/49)	69.4% (34/49)	90.0% (36/40)	77.5% (31/40)	97.7% (42/43)	91.9% (34/37)	0.41 ± 0.19
3000	83.7% (41/49)	65.3% (32/49)	90.0% (36/40)	70.0% (28/40)	93.2% (41/44)	94.1% (32/34)	0.49 ± 0.21
4000	75.5% (37/49)	57.1% (28/49)	80.0% (32/40)	60.0% (24/40)	94.9% (37/39)	93.3% (28/30)	0.68 ± 0.23
5000	65.3% (32/49)	36.7% (18/49)	65.0% (26/40)	37.5% (15/40)	86.5% (32/37)	75.0% (18/24)	0.77 ± 0.27

ADC, apparent diffusion coefficient; PPV, positive predictive value.

TABLE 3. *P*-values From Comparison of Image Sets with Respect to Measures of Reader Performance

Sensitivity (All Tumors)

	ADC	b1000	b1500	b2000	b2500	b3000	b4000
b1000	R1: 0.654 R2: 0.282	—	—	—	—	—	—
b1500	R1: 0.413 R2: 0.526	R1: 0.254 **R2: 0.028r**	—	—	—		—
b2000	R1: 0.176 R2: 1.000	R1: 0.098 R2: 0.151	R1: 0.313 R2: 0.412	—	—	—	—
b2500	R1: 0.314 R2: 0.739	R1: 0.175 R2: 0.252	R1: 1.000 R2: 0.252	R1: 0.313 R2: 0.313	—	—	—
b3000	R1: 0.705 R2: 0.363	R1: 0.479 R2: 0.763	R1: 0.313 R2: 0.089	R1: 0.151 R2: 0.252	R1: 0.563 R2: 0.412	—	—
b4000	R1: 0.253 **R2: 0.029c**	R1: 0.478 R2: 0.363	**R1: 0.021c** **R2: 0.001c**	**R1: 0.011c** **R2: 0.005c**	**R1: 0.021c** **R2: 0.028c**	**R1: 0.039c** R2: 0.095	—
b5000	**R1: 0.009c** **R2: <0.001c**	**R1: 0.016c** **R2: 0.002c**	**R1: 0.006c** **R2: <0.001c**	**R1: 0.002c** **R2: <0.001c**	**R1: 0.003c** **R2: <0.001c**	**R1: 0.010c** **R2: <0.001c**	R1: 0.089 **R2: 0.002c**

Sensitivity (Gleason Score > 6)

	ADC	b1000	b1500	b2000	b2500	b3000	b4000
b1000	R1: 0.654 R2: 0.364	—	—	—	—	—	—
b1500	**R1: 0.042r** R2: 0.478	**R1: 0.023r** R2: 0.052	—	—	—	—	—
b2000	**R1: 0.042r** R2: 0.705	**R1: 0.023r** R2: 0.094	R1: 1.000 R2: 0.654	—	—	—	—
b2500	R1: 0.077 R2: 0.705	**R1: 0.040r** R2: 0.094	R1: 0.313 R2: 0.654	R1: 0.313 R2: 1.000	—	—	—
b3000	R1: 0.177 R2: 0.526	R1: 0.100 R2: 0.739	R1: 0.313 R2: 0.095	R1: 0.313 R2: 0.173	R1: 1.000 R2: 0.173	—	—
b4000	R1: 0.654 R2: 0.051	R1: 1.000 R2: 0.313	**R1: 0.023c** **R2: 0.002c**	**R1: 0.001c** R2 <0.001c	**R1: 0.040c** **R2: 0.005c**	**R1: 0.040c** **R2: 0.037c**	—
b5000	**R1: 0.015c** **R2: <0.001c**	**R1: 0.028c** **R2: 0.001c**	**R1: 0.001c** **R2: <0.001c**	**R1: 0.001c** **R2: 0.001c**	**R1: 0.001c** **R2: <0.001c**	**R1: 0.001c** **R2: <0.001c**	**R1: 0.010c** **R2: 0.001c**

ADC, apparent diffusion coefficient.

Values listed in bold when statistically significant at p<0.05. For statistically significant differences, "r" and "c" are used to denote whether the image set represented by the given row or column, respectively, had higher sensitivity.

1500 and 2000 in comparison with the ADC map. In addition, PPV for tumor was similar across most b-values for both readers, although lower at a b-value of 5000 for reader 1 and at b-values of 1000 and 5000 for reader 2.

Quantitative tumor-to-prostate contrast showed a significant increase with increasing b-value ($r = +0.69$, $P < 0.001$) (Table 2).

Figures 1 and 2 demonstrate representative patients. Figure 3 graphically summarizes trends in anatomic clarity, tumor-to-PZ contrast, and reader sensitivity across b-values.

DISCUSSION

We compared the accuracy for tumor detection of computed DWI using a wide range of b-values. Consistent with previous studies (12,16), accuracy initially improved significantly when increasing the b-value past 1000 s/mm^2, attributed to increasing background prostate tissue suppression. However, there is a paucity of data regarding the diagnostic impact of extremely high b-values. As would be expected, background signal suppression progressively increased with increasing b-values. However, this phenomenon provided diminishing benefit at the highest investigated b-values owing to eventual excessive lose of signal within the prostate and surrounding tissues, leading to diminished anatomic clarity and diminished visualization of normal landmarks such as the prostate capsule and PZ-TZ edge. This effect at the highest b-values may have led to difficulty in tumor location, thereby providing an explanation for the observed decreases in reader performance at b-values in the range of 3000–5000 s/mm^2.

Based on our data, it is not possible to favor a single b-value as optimal (ie, as achieving highest diagnostic performance, when considering both sensitivity and PPV) in comparison with the others given comparable performance of a number of the consecutive b-values. However, in consideration of the data, a b-value in the range of 1500–2500 s/mm^2 appears to

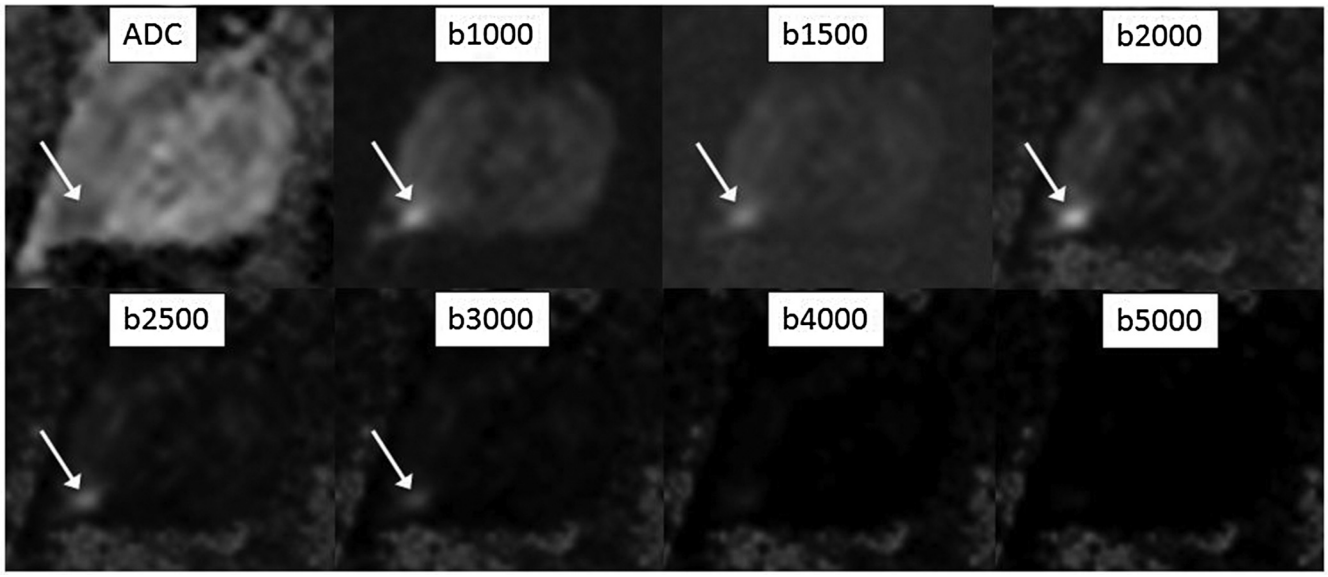

Figure 1. A 64-year old man with Gleason score 3 + 4 tumor in the right posterolateral peripheral zone at radical prostatectomy that shows decreased apparent diffusion coefficient (ADC) (arrows). Tumor is best visualized relative to surrounding prostate tissue at intermediate b-values.

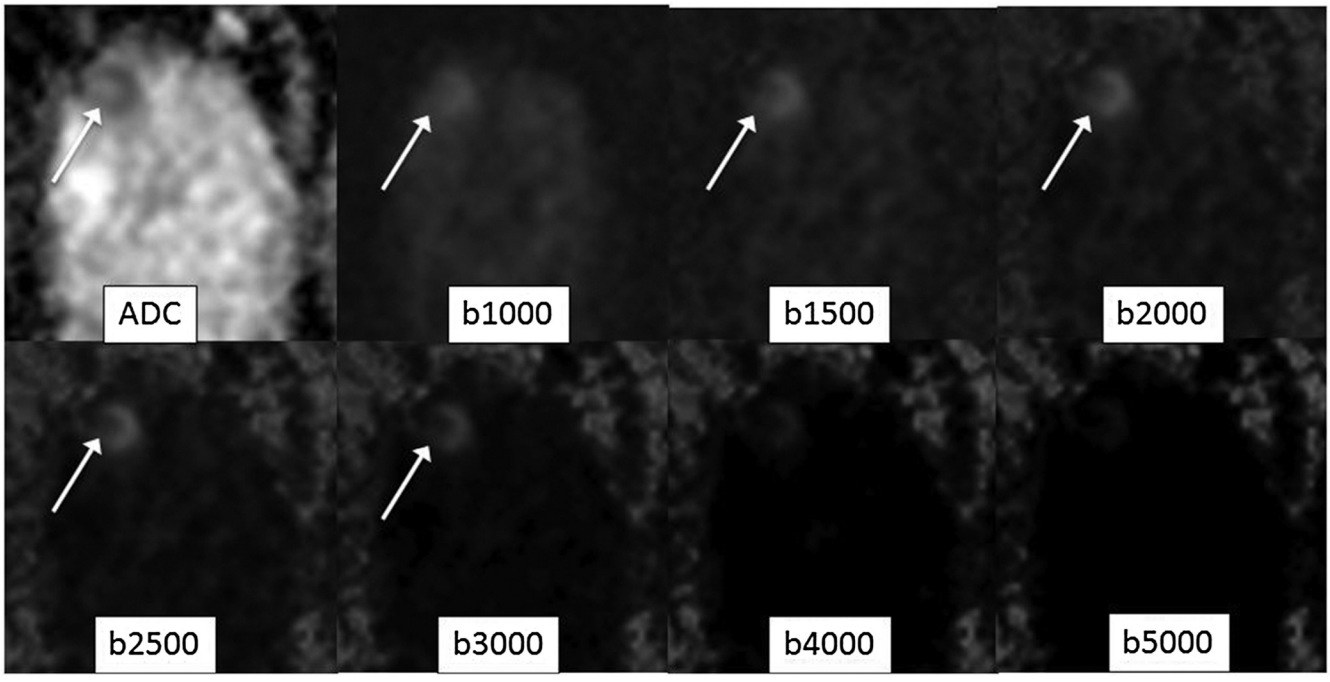

Figure 2. An 80-year old man with Gleason score 3 + 4 tumor in the right anterior transition zone at radical prostatectomy that shows decreased apparent diffusion coefficient ADC (arrows). Tumor is best visualized relative to surrounding prostate tissue at intermediate b-values.

be optimal, with similar excellent performance observed for both readers across this range, and decreased performance to a varying degree between readers at even higher b-values. While an individual b-value within this range cannot be specifically advised for clinical practice, our findings do highlight the importance of incorporating high b-value images within this range into routine prostate MRI interpretation, as is also advised by PI-RADS v2 (1). Such b-values heavily outperformed the images obtained using a b-value of 1000 for both readers, and to a lesser extent outperformed the ADC map as well. At present, only certain MRI systems include the ability to perform computed DWI in combination with clinically available DWI sequences. In addition, while software packages can be used to retrospectively perform computed DWI, such packages are not available at many centers and also may be more difficult to integrate into clinical workflows

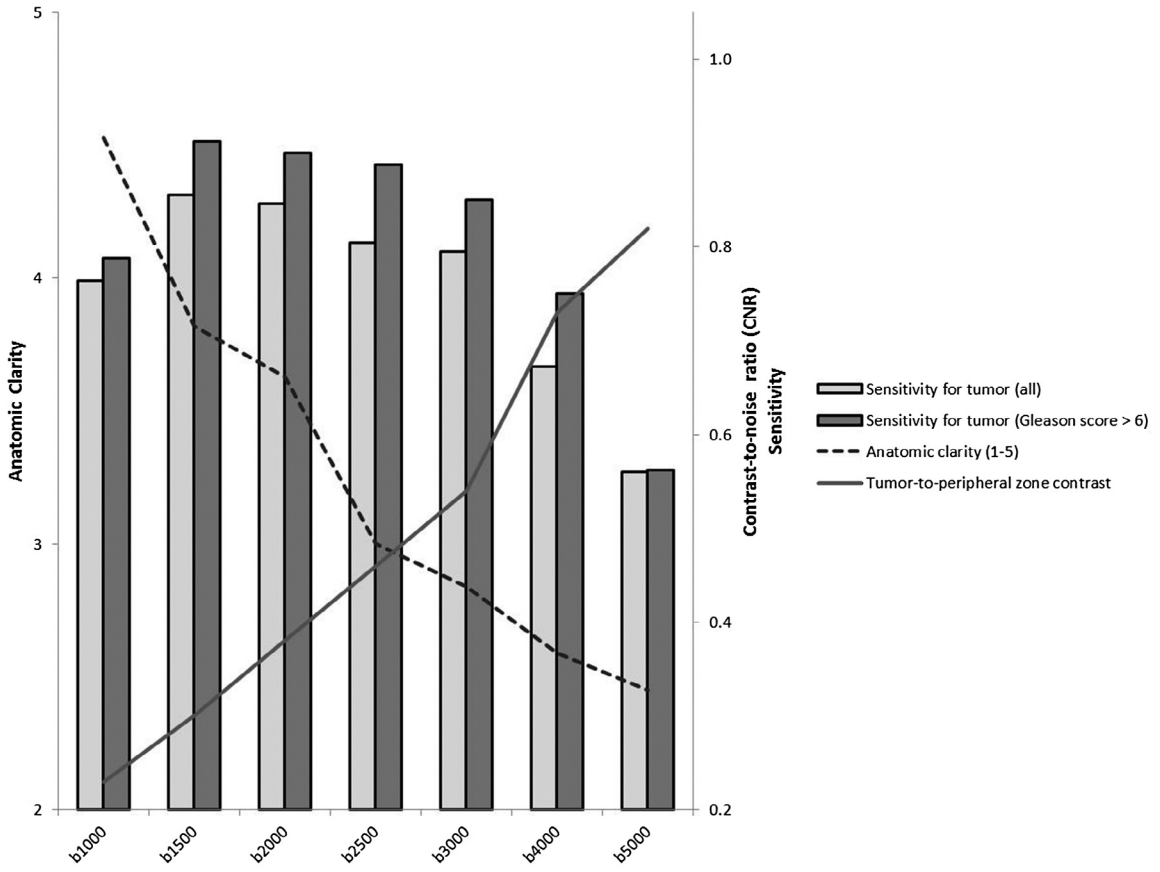

Figure 3. Graphical summary of trends in anatomic clarity, tumor-to-peripheral zone (PZ) contrast, and reader sensitivity across b-values. Results of the two readers are averaged for illustrative purposes.

in order to allow for incorporation of computed DWI into formal interpretations. When software is available for dynamic or interactive generation of computed b-value DWI, one interesting idea would be to simultaneously evaluate an array of computed very high b-values, rather than a single computed b-value, in an effort to integrate the benefits of the various b-values (ie, better anatomic clarity vs better background signal suppression), without requiring additional acquisition time.

Feuerlein et al. also evaluated computed DWI in prostate tumors at b-values up to 4000 s/mm^2, reporting increased qualitative and quantitative tumor conspicuity at the highest b-values (11). However, their study sample comprised 14 patients having undergone prostate biopsy, which was not sufficient to perform a meaningful assessment of diagnostic reader accuracy (11). Moreover, these past authors anecdotally acknowledged limitations of the highest b-values, noting extreme variations in signal intensity in normal structures, including periprostatic tissues, at the highest b-values (11). Such signal intensity variation was accounted for by the error propagation theory (9) and suggested to be a source of potential difficulty during clinical image evaluation (11). In addition, Vural et al. evaluated computed DWI of prostate cancer at b-values up to 3000 s/mm^2 in 29 patients using consensus interpretations (17). These authors reported better background tissue suppression and tumor contrast ratios at the b-value of 3000 s/mm^2, yet better zonal delineation and similar tumor detection rate at a b-value of 2000 s/mm^2, such that a b-value of 2000 s/mm^2 was selected as preferable. Such trends are consistent with the overall pattern of findings within our study.

Our study has a number of limitations. First, the study was retrospective and did not have a large sample size. Second, the computation of the very high b-values using a standard mono-exponential model precludes assessment of the non-Gaussian properties of tissue diffusion, as can be evaluated by applying a diffusion kurtosis model to the directly acquired very high b-value images (18). The diffusion kurtosis model is hypothesized to better reflect heterogeneity of tissue microstructure and influences of the intracellular environment, which may have particular value for detecting cellular, high-grade tumors (19). However, the impact of this potential loss of information through the use of computed very high b-values was not explored in our study. Moreover, a recent study showed the feasibility of performing computed DWI using non-mono-exponential models, such as the non-Gaussian kurtosis model or the intra-voxel incoherent motion model (16). Although we did not investigate such models in our study, the earlier study did not demonstrate a clear diagnostic benefit

from use of these other models in comparison with acquired DWI (16). Likewise, the mono-exponential model does not reflect perfusion contributions to the measured SI, as are assessed by the intravoxel incoherent motion model of diffusion behavior (20). Such perfusion effects would be anticipated to be non-negligible at the low acquired b-value of 50 s/mm^2 in our study. Third, we did not perform separate analyses for peripheral and transition zone tumors given the small number of transition zone tumors in our cohort. Fourth, we were unable to report specificity for tumor detection given the analysis on a per-lesion basis, in which true-negative findings are undefined. However, we have reported PPV as a reflection of the frequency of false-positive interpretations. Fifth, we only evaluated computed DWI obtained using a single software platform. It is possible that performance of computed DWI at very high b-values depends on aspects of the algorithm used (for instance, the handling of potentially negative voxel values at increasing b-values), and that findings may be different when using other platforms. Sixth, we did not evaluate the diagnostic performance of multiple different b-values being assessed in a joint fashion, possibly also in combination with the ADC map. Seventh, although the computed high b-value images compared favorably with the ADC map, the ADC map has the additional established role in providing a quantitative biomarker of tumor aggressiveness, which is not achieved using the high b-value images. In this regard, we acknowledge that computed DWI's primary role in practice seems to be to aid the visual detection of suspicious regions during clinical interpretation, although not to replace the ADC map itself. Finally, the readers in our study were aware that all patients had undergone radical prostatectomy for prostate cancer, thereby influencing their interpretations for the presence of tumor. The relative impact of computed very high b-value DWI for initial prostate cancer detection is unknown from our study.

In conclusion, computed b-values in the range of 1500–2500 s/mm^2 were optimal for prostate cancer detection. In comparison, b-values of 1000 or 3000–5000 s/mm^2 exhibited lower performance, relating to insufficient signal suppression at the low b-value and excessive signal suppression leading to diminished anatomic clarity at the higher b-values. Given the findings, widespread availability of computed DWI with b-values in the range of 1500–2500 s/mm^2 across clinical magnetic resonance platforms should be considered a priority for optimizing prostate MRI interpretation.

ACKNOWLEDGMENTS

We would like to thank the Joseph and Diane Steinberg Charitable Trust.

REFERENCES

1. American College of Radiology. Magnetic Resonance Prostate Imaging Reporting and Data System (MR PI-RADS). Available at: http://www.acr.org/Quality-Safety/Resources/PIRADS. Accessed May 21, 2015.
2. Rosenkrantz AB, Kong X, Niver BE, et al. Prostate cancer: comparison of tumor visibility on trace diffusion-weighted images and the apparent diffusion coefficient map. AJR Am J Roentgenol 2011; 196:123–129.
3. Rosenkrantz AB, Chandarana H, Hindman N, et al. Computed diffusion-weighted imaging of the prostate at 3 T: impact on image quality and tumour detection. Eur Radiol 2013; 23:3170–3177.
4. Barth BK, Cornelius A, Nanz D, et al. Diffusion-weighted imaging of the prostate: image quality and geometric distortion of readout-segmented versus selective-excitation accelerated acquisitions. Invest Radiol 2015; 50:785–791.
5. Korn N, Kurhanewicz J, Banerjee S, et al. Reduced-FOV excitation decreases susceptibility artifact in diffusion-weighted MRI with endorectal coil for prostate cancer detection. Magn Reson Imaging 2015; 33:56–62.
6. Donato F, Jr, Costa DN, Yuan Q, et al. Geometric distortion in diffusion-weighted MR imaging of the prostate-contributing factors and strategies for improvement. Acad Radiol 2014; 21:817–823.
7. Blackledge MD, Leach MO, Collins DJ, et al. Computed diffusion-weighted MR imaging may improve tumor detection. Radiology 2011; 261:573–581.
8. Ueno Y, Takahashi S, Ohno Y, et al. Computed diffusion-weighted MRI for prostate cancer detection: the influence of the combinations of b-values. Br J Radiol 2015; 88:20140738.
9. Maas MC, Futterer JJ, Scheenen TW. Quantitative evaluation of computed high B value diffusion-weighted magnetic resonance imaging of the prostate. Invest Radiol 2013; 48:779–786.
10. Bittencourt LK, Attenberger UI, Lima D, et al. Feasibility study of computed vs measured high b-value (1400 s/mm(2)) diffusion-weighted MR images of the prostate. World J Radiol 2014; 6:374–380.
11. Feuerlein S, Davenport MS, Krishnaraj A, et al. Computed high b-value diffusion-weighted imaging improves lesion contrast and conspicuity in prostate cancer. Prostate Cancer Prostatic Dis 2015; 18:155–160.
12. Rosenkrantz AB, Hindman N, Lim RP, et al. Diffusion-weighted imaging of the prostate: Comparison of b1000 and b2000 image sets for index lesion detection. J Magn Reson Imaging 2013; 38:694–700.
13. Cornfeld DM, Israel G, McCarthy SM, et al. Pelvic imaging using a T1W fat-suppressed three-dimensional dual echo Dixon technique at 3T. J Magn Reson Imaging 2008; 28:121–127.
14. Rosenkrantz AB, Neil J, Kong X, et al. Prostate cancer: Comparison of 3D T2-weighted with conventional 2D T2-weighted imaging for image quality and tumor detection. AJR Am J Roentgenol 2010; 194:446–452.
15. Hubbard AE, Ahern J, Fleischer NL, et al. To GEE or not to GEE: comparing population average and mixed models for estimating the associations between neighborhood risk factors and health. Epidemiology 2010; 21:467–474.
16. Grant KB, Agarwal HK, Shih JH, et al. Comparison of calculated and acquired high b value diffusion-weighted imaging in prostate cancer. Abdom Imaging 2015; 40:578–586.
17. Vural M, Ertas G, Onay A, et al. Conspicuity of peripheral zone prostate cancer on computed diffusion-weighted imaging: comparison of cDWI1500, cDWI2000, and cDWI3000. Biomed Res Int 2014; 2014:768291.
18. Rosenkrantz AB, Sigmund EE, Johnson G, et al. Prostate cancer: feasibility and preliminary experience of a diffusional kurtosis model for detection and assessment of aggressiveness of peripheral zone cancer. Radiology 2012; 264:126–135.
19. Rosenkrantz AB, Padhani AR, Chenevert TL, et al. Body diffusion kurtosis imaging: Basic principles, applications, and considerations for clinical practice. J Magn Reson Imaging 2015; 42:1190–1202.
20. Shinmoto H, Tamura C, Soga S, et al. An intravoxel incoherent motion diffusion-weighted imaging study of prostate cancer. AJR Am J Roentgenol 2012; 199:W496–W500.